LUNAR STRUCTURE AND DYNAMICS - RESULTS FROM THE APOLLO PASSIVE SEISMIC EXPERIMENT*

GARY LATHAM, MAURICE EWING, JAMES DORMAN,
YOSIO NAKAMURA
The University of Texas at Galveston, Tex., U.S.A.
FRANK PRESS, NAFI TOKSŐZ,
Massachusetts Institute of Technology, Cambridge, Mass., U.S.A.
GEORGE SUTTON, FRED DUENNEBIER,
University of Hawaii H.I., U.S.A.
and
DAVID LAMMLEIN
Lamont-Doherty Geological Observatory, Columbia University, Palisades, N.Y., U.S.A.

(Received 29 November, 1972)

Abstract. Analysis of seismic signals from man-made impacts, moonquakes, and meteoroid impacts has established the presence of a lunar crust, approximately 60 km thick in the region of the Apollo seismic network; an underlying zone of nearly constant seismic velocity extending to a depth of about 1000 km, referred to as the mantle; and a lunar core, beginning at a depth of about 1000 km, in which shear waves are highly attenuated suggesting the presence of appreciable melting. Seismic velocitites in the crust reach 7 km s^{-1} beneath the lower-velocity surface zone. This velocity corresponds to that expected for the gabbroic anorthosites found to predominate in the highlands, suggesting that rock of this composition is the major constituent of the lunar crust. The upper mantle velocity of about 8 km s^{-1} for compressional waves corresponds to those of terrestrial olivines, pyroxenites and peridotites. The deep zone of melting may simply represent the depth at which solidus temperatures are exceeded in the lower mantle. If a silicate interior is assumed, as seems most plausible, minimum temperatures of between 1450°C and 1600°C at a depth of 1000 km are implied. The generation of deep moonquakes, which appear to be concentrated in a zone between 600 km and 1000 km deep, may now be explained as a consequence of the presence of fluids which facilitate dislocation. The preliminary estimate of meteoroid flux, based upon the statistics of seismic signals recorded from lunar impacts, is between one and three orders of magnitude lower than previous estimates from Earth-based measurements.

1. Introduction

With the successful installation of a geophysical station at the Descartes landing site of Apollo mission 16 in April, 1972, a 4-station lunar seismic network was completed. It spans the near face of the Moon in an approximate equilateral triangle with 1100 km spacing between stations. Continued operation of the Apollo seismic network over a period of several years will provide data necessary to deduce the gross structure and dynamics of the lunar interior, and the present flux of meteoroids in the vicinity of the Earth. This paper describes progress toward these objectives as of September, 1972.

* Paper dedicated to Professor Harold C. Urey on the occasion of his 80th birthday on 29 April, 1973.

The Moon 7 (1973) 396–420.

Station 16 appears to be the most sensitive of the four lunar seismograph stations. Based upon the initial 45-day period of operation, seismic events are recorded at station 16 at an average rate of 10000 per year. Most of these events are moonquakes. This compares with rates of 2000 events per year at station 14, and 700 events per year at stations 12 and 15. The signal character and background noise at each station have distinctive characteristics apparently related to the depth and elastic properties of the regolith at each site. To explain these differences, station 16 must have the deepest and/or weakest regolith according to criteria now applied. This would also explain the much higher sensitivity of station 16.

The largest signal recorded in the three years of observation since the installation of the Apollo 12 station occurred on May 13, 1972. It was generated by a meteoroid impact approximately 139 km north of station 14 and was well recorded by all stations of the Apollo seismic network. We presently estimate the mass of this meteoroid at approximately 1100 kg. The statistics of impacts detected at station 12 over a 399-day period indicate the probability of an impact of this size to be about one every ten years for the entire Moon.

Significant progress in the measurement of meteoroid flux in near-earth space, determination of lunar structure, and the delineation of active moonquake source regions have been made. It now appears that moonquakes are concentrated at great depth (600–1000 km) and that the apparent disparity between meteoroid flux estimates based upon lunar crater counts and those from earth-based observations may be resolved by seismic measurements in favor of the lower flux indicated by the crater-count method. From preliminary analysis of seismic signals from a large far-side impact and from two far-side moonquakes, it appears that melting begins in the present-day Moon at a depth of about 1000 km, i.e., just beneath the zone of moonquake activity.

2. Instrument Description and Performance

A seismometer consists simply of a mass that is free to move in one direction and that is suspended by means of a spring (or a combination of springs and hinges) from a framework. The suspended mass is provided with damping to suppress vibrations at the natural frequency of the system. The framework rests on the surface, the motions of which are to be studied, and moves with the surface. The suspended mass tends to remain fixed in space because of its own inertia, while the frame moves in relation to the mass. The resulting relative motion between the mass and the framework can be recorded and used to calculate original ground motion if the instrument constants are known.

The Apollo seismic stations consist of two main subsystems: the sensor unit and a separate electronics module incorporated into the central transmitting station. The sensor unit, shown schematically in Figure 1, contains three matched long-period (LP) seismometers (with resonant periods of 15 s) aligned orthogonally to measure one vertical (Z) and two horizontal (X and Y) components of surface motion. The sensor unit also includes a short-period (SP) seismometer (with a resonant period of 1 s) that

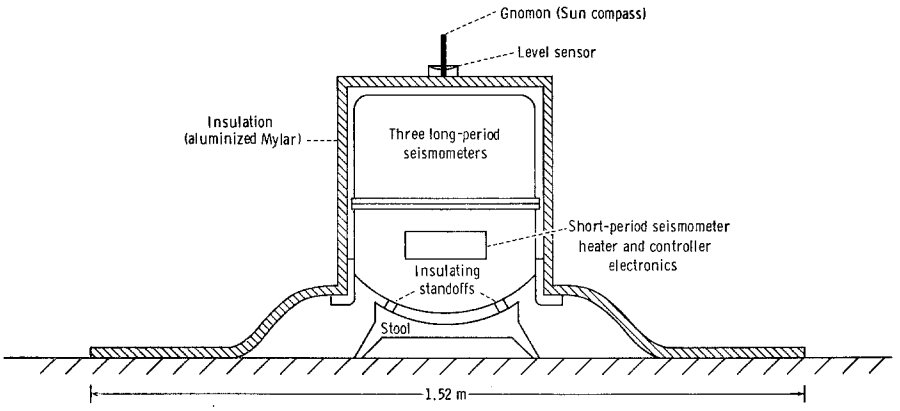

Fig. 1. Schematic diagram of seismic sensor system.

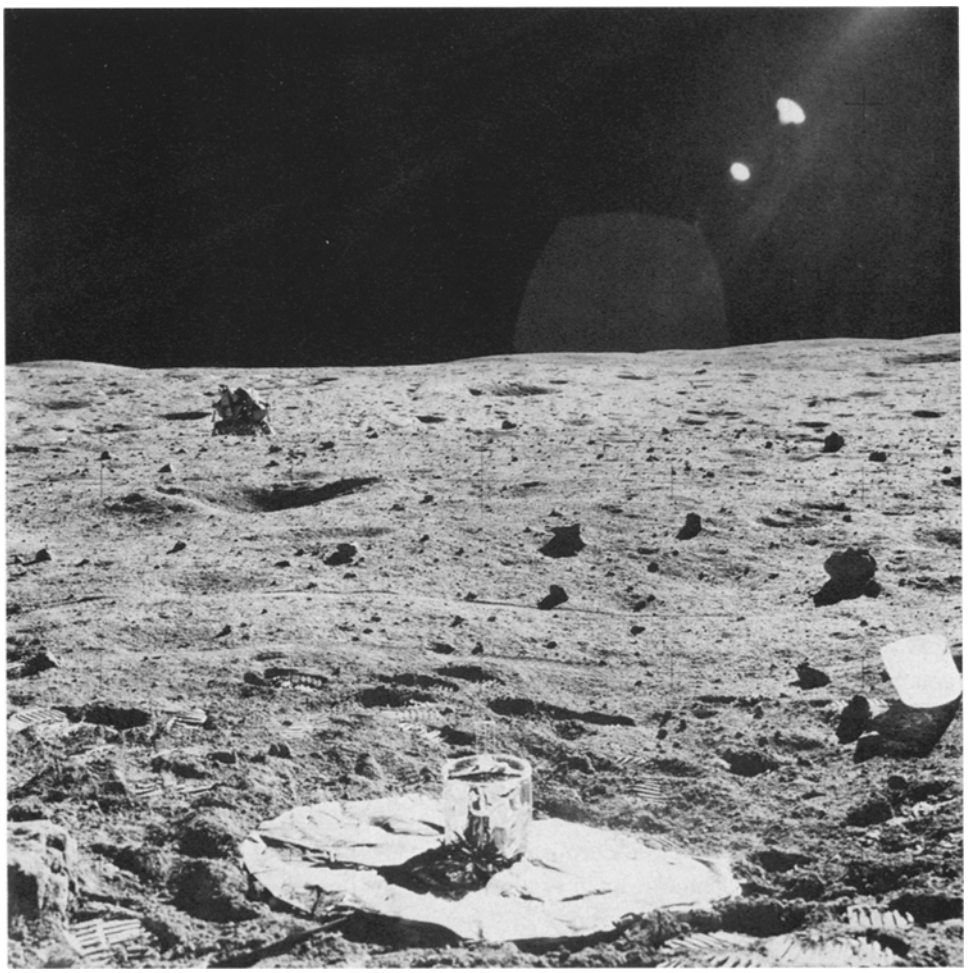

Fig. 2. Apollo 16 seismometer after deployment on the lunar surface.

is sensitive to vertical motion at higher frequencies. The instrument is constructed principally of beryllium and weighs 11.5 kg, including the electronics module and thermal insulation. Without insulation, the sensor unit is 23 cm in diameter and 29 cm high. The total power drain varies between 4.3 and 7.4 W.

Instrument temperature control is provided by a 6-W heater, a proportional controller, and an aluminized Mylar insulating shroud. The shroud also extends over the local surface to reduce temperature variations of the surface material.

The LP horizontal-component (LPX and LPY) seismometers are very sensitive to tilt and are leveled to high accuracy by means of a two-axis, motor-driven gimbal. A third motor adjusts the LP vertical-component (LPZ) seismometer in the vertical direction. Motor operation is controlled by command. Calibration of the complete system is accomplished by applying an accurate increment or step of current to the coil of each of the four seismometers by transmission of a command from Earth. The current step is equivalent to a known step of ground acceleration.

During transport and deployment, a pneumatic caging system is used in which pressurized bellows expand to clamp fragile parts in place. Uncaging is performed on command by releasing the compressed gas by means of a small explosive device.

The seismometer system is controlled from Earth by 15 commands that govern such functions as speed and direction of leveling motors, instrument gain, and calibration. The Apollo 16 seismometer is shown fully deployed on the lunar surface in Figure 2.

Two modes of operation of the LP seismometers are possible: the flat-response mode and the peaked-response mode. In the flat-response mode, the seismometers have natural periods of 15 s and can detect ground motions as small as 0.3 nm over the frequency range from 0.1 Hz to 1 Hz. In the peaked-response mode, the seismometers act as underdamped pendulums with natural periods of 2.2 s. Maximum sensitivity is increased by a factor of 5.6 in the peaked-response mode, but sensitivity to low-frequency signals is reduced. The SP seismometer can detect ground motions of 0.3 nm at 1 Hz with peak sensitivity at 8 Hz. The seismometer response curves are shown in Figure 3.

Episodes of seismic disturbances are observed on the LP seismometers of all seismic stations throughout the lunar day. These disturbances are most intense near times of terminator passage and are believed to be caused by thermal contraction and expansion of the Mylar thermal shroud that blankets the sensor and the cable connecting the sensor with the central station.

3. Results and Discussion

A. SEISMIC SIGNAL CHARACTERISTICS AND WAVE TRANSMISSION IN THE MOON

As has been described in previous papers [4–11, 24], the characteristics of lunar seismograms differ markedly from those of typical Earth recordings. The most striking feature of lunar signals is their duration. Signals from the impacts of the S-IVB stages of the Apollo boosters, for example, last for several hours. On Earth, signal durations under equivalent conditions would be measured in minutes. Lunar signals have emer-

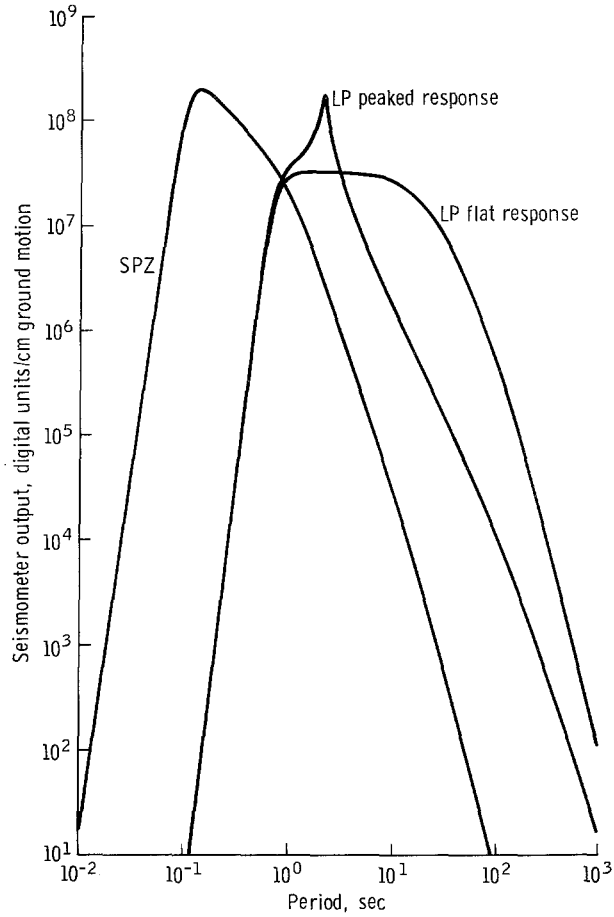

Fig. 3. Response curves for the LP and SP vertical-component seismometers. The ordinate scale is in digital units (DU) per centimeter ground displacement amplitude. A DU is the signal variation that corresponds to a change in the least significant bit of the 10-bit data word.

gent beginnings, increase gradually to a maximum, and then slowly decay. Following the first one or two cycles of initial P-wave motion, the ground motion becomes so complex that there is little or no correlation between any two components. The onset of direct shear waves are indistinct where they can be identified at all. Typical dispersed surface wave trains have not been recognized in any of the signals recorded to date; although, surface wave energy undoubtedly contributes to the signal as will be shown below. Thus, many of the analysis techniques found useful in terrestrial seismology cannot be applied to lunar signals. For example, it is rarely possible to determine the direction of propagation from the particle motion at a single station. These and other unusual characteristics of the lunar seismic signals, have been interpreted as resulting from intensive, but nearly loss-free, scattering of seismic waves in a heterogeneous layer that blankets the entire surface of the Moon [7, 9, 24]. The low seismic velocity of this layer makes the lunar surface a strong wave guide. Below this surface layer, the

seismic velocity increases markedly and the lunar material is believed to be sufficiently homogeneous to transmit seismic waves with little scattering. In this structure, seismic waves generated by an impacting object are intensively scattered near the impact point and are observed as a scattered wavetrain in the near ranges. A part of the scattered energy gradually leaks into the lunar interior where it propagates as a long train of seismic waves, undergoes further scattering when it reenters the lunar surface layer, and is observed as a prolonged wavetrain at a distant seismic station. Since both compressional and shear waves are transmitted in the lunar interior, separation of the wavetrain into two components which begin at different times is expected at far ranges.

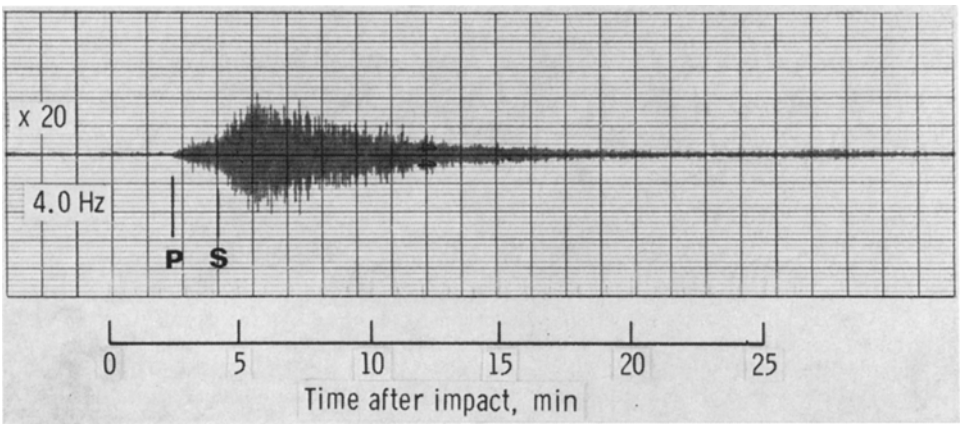

Fig. 4. Seismic signals from Apollo 16 S-IVB impact observed by the station 15 SPZ seismometer at a distance of 1100 km. The signal has been narrow-band filtered with a center frequency of 4.0 Hz.

Figure 4 shows a typical seismic waveform observed at far ranges, reproduced through a narrow bandpass filter. The partial separation of two wavetrains, each having a characteristic envelope of a scattered wavetrain, is easily seen. The scattered P-wave train begins about 2.5 min after impact. The scattered S-wave train arrives about 1.8 min after the beginning of the P-wave train with maximum amplitude about three times that of the P-wave train. No other arrivals are apparent at least for seismic waves at this frequency (4 Hz).

In Figure 5 the travel times to the peak of the signal envelope as measured on narrow-band filtered seismograms are plotted against distance.

Three characteristics of these curves are relevant to this discussion: (1) the rise times of seismic signals (time to reach maximum amplitude) increase with distance, but the slopes of the curves decrease markedly at a range of about 100 km to 150 km depending upon frequency; (2) signal rise times at far ranges begin to increase sharply as the frequency falls below 1 Hz; and (3) a prominent dip in rise times occurs at all frequencies at a range of approximately 180 km, but is most pronounced at low frequencies. These characteristics are consistent with the scattering-layer hypothesis described above.

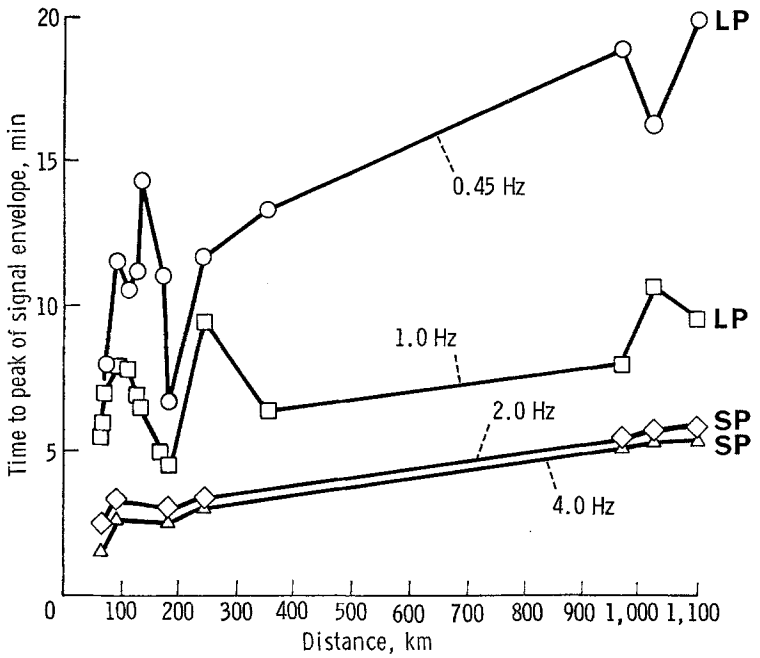

Fig. 5. Observed time intervals from the times of impact to the peak of the seismic signal envelope for artificial impacts. Data for the meteoroid impact of May 13, 1972, are included at distances of 967 km and 1026 km. The time intervals are measured on narrow-band filtered seismograms of LP (0.45 Hz and 1.0 Hz) and SPZ (2 Hz and 4 Hz) components.

Let us consider the propagation of seismic wave energy from an impact in the postulated structure in greater detail. Seismic energy will radiate outward from the point of impact as body waves (compressional and shear waves), which travel through the lunar interior; and as surface waves, which travel along the surface. Surface waves will carry most of the energy initially because of the wave guide effect and efficient generation by a surface source. Surface waves with wavelengths comparable to the thickness of the scattering zone, and shorter, are quickly scattered into secondary surface waves and body waves [26]. Partitioning of scattered surface wave energy probably favors secondary surface waves. Therefore, conversion to body waves provides a path by which energy may gradually 'leak' into the lunar interior. Longer surface waves can propagate to greater ranges. The relative contributions of body and surface waves to the maximum amplitude of the detected wavetrain thus depends upon range and frequency. According to the present hypothesis, the contributions at ranges of less than 100 to 150 km, are mainly primary and secondary surface waves. Thus, scattering will increase with path length and a pronounced change in signal rise time with distance is to be expected in this range. At longer ranges, gradual separation of the wave types as a result of their differing velocities, results in the dominance of shear waves at higher frequencies and surface waves at lower frequencies. From the data shown in Figure 5, it appears that the signal frequency for which surface waves begin

to dominate at long ranges is about 0.5 Hz, with shear waves dominant at frequencies of 1 Hz and higher. At ranges greater than 100 km, little further scattering of body waves occurs since most of their path is below the scattering zone. Thus, the signal rise times change relatively little beyond this range for frequencies of 1 Hz and higher. However, for lower frequencies (0.5 Hz and lower), in which surface wave energy is dominant, the effect of scattering decreases gradually as wavelength increases. Thus, signal rise times continue to increase markedly with range beyond 150 km at low frequencies. Surface waves (Rayleigh waves of the fundamental mode) have wavelengths of about 1 km at a frequency of 0.5 Hz for the assumed structure. From this, we conclude that most of the scattering occurs in the upper few hundred meters of the surface layer.

The dip in the rise time curves at a range of 180 km is caused by focussing of body waves which contribute to a rapid buildup in signal intensity at this range. Body wave focussing at a range of 180 km is in accord with theoretical calculations for a model containing a discontinuity at a depth of about 60 km (the crust-mantle boundary). Thus, the rise-time data provide independent evidence in support of the model derived in the section entitled Lunar Structure.

Our hypothesis that the lunar interior transmits seismic waves with little scattering implies that, once a seismic wave train leaves the surface scattering layer, its envelope shape is preserved while it propagates through the lunar interior. Shear waves play the major role in determining the high-frequency peak of the signal envelope observed in the far ranges as discussed above. Therefore, the apparent velocity of the envelope peak along the lunar surface in the far ranges, measureable from Figure 5, is expected to represent the apparent velocity of shear waves in this range. The velocity thus determined for signals in the frequency range from 2 Hz to 4 Hz is 5.0 km s^{-1}. Correcting for the curvature of the lunar surface, this corresponds to a true shear-wave velocity in the upper mantle of the Moon of 4.7 km s^{-1}. By combining this value with the compressional-wave velocity of 8.1 km s^{-1}, we obtain an estimated value of 0.25 ± 0.02 for the Poisson's ratio of the material in the upper mantle of the Moon. This is consistent with the presence of temperatures well below the solidus at these depths.

The processes that have led to the formation of the surficial zone in which intensive scattering of seismic waves occurs, referred to here as the scattering zone, have undoubtedly been varied and complex. However, meteoroid impacts have probably been the dominant agent. Volcanic processes, including fracturing of lavas by cooling shrinkage, may have contributed to the seismic heterogeneity of the zone. The very low attenuation of seismic waves in the scattering zone is probably a consequence of the lack of volatiles in the material.

B. LUNAR STRUCTURE

Information on lunar structure to a depth of about 120 km has been obtained primarily from the seismic signals generated by the LM and S-IVB impacts of Apollo missions 12, 14, 15, and 16. Structural information at greater depths derives from deep moon-

quake signals and from the relatively rare, large meteoroid impacts detectable at ranges greater than 1000 km. With the exception of mission 16, the times and locations of the LM and S-IVB impacts are precisely known from NASA tracking data. Premature loss of tracking resulted in a degraded estimate of impact parameters for the Apollo 16 S-IVB; and the retrofire ignition required for the impact of the Apollo 16 LM was not accomplished. In three cases (Apollo 13 and 14 S-IVB's, and Apollo 14 LM), features believed to be the impact craters have been identified in surface photographs (personal communications, Ewen A. Whitaker, 1972).

The time and location of Apollo 16 S-IVB impact were determined from the travel times of seismic waves to stations 12 and 14 by utilizing the travel-time data obtained from previous impacts. The large meteoroid impact of May 13, 1972, gave clearly

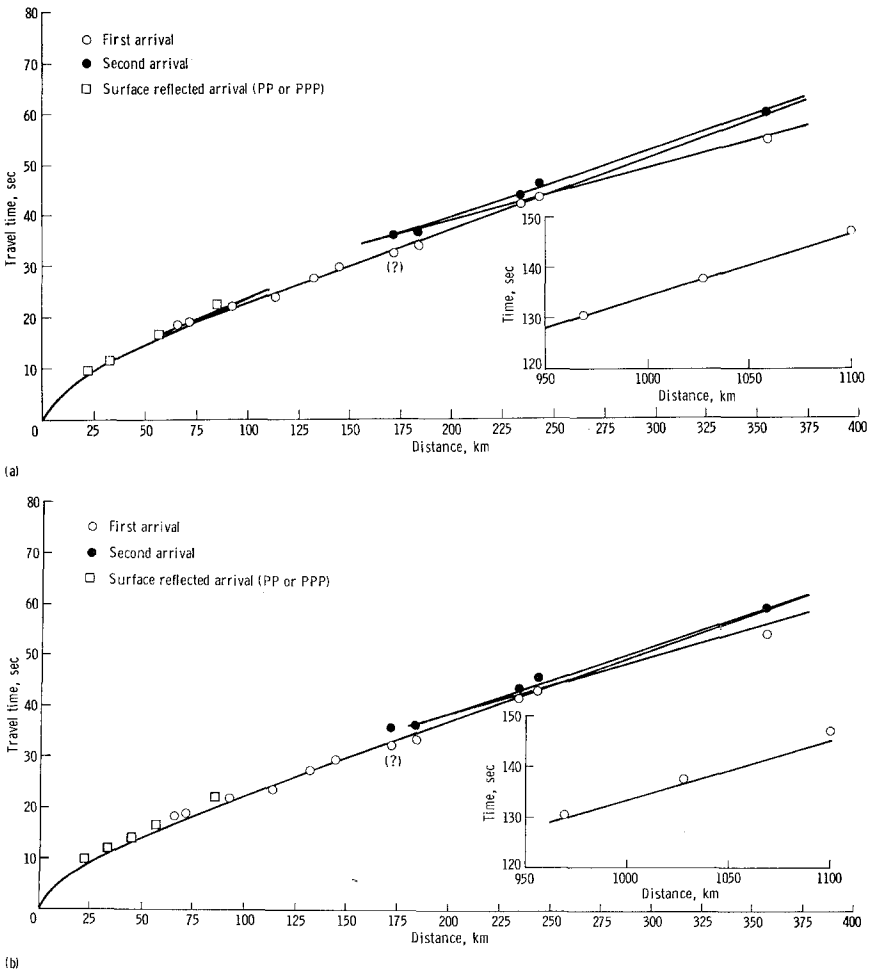

Fig. 6. Travel time observations and theoretical curves for two models. Upper figure is a composite of models LM-1 and LM-3. Lower figure is LM-2. Data are all P-wave travel-time observations. Second arrival means large amplitude wave following the refracted arrival. Surface reflected arrivals are PP or PPP phases, plotted at one half or one third the source-receiver distance, respectively.

identifiable P-waves at all four stations of the Apollo seismic network and was also located by travel-time methods. These data provide an independent check on the lunar model previously determined.

1. *The Crust and Upper Mantle of the Moon*

Travel time data available from the LM and S-IVB impacts through mission 16 and the meteoroid impact of May 13, 1972, are shown in Figure 6. We should emphasize that the travel times to stations 12 and 14 from neither the S-IVB impact of mission 16 nor the meteoroid impact provide independent information on lunar structure since the data from these stations were used with existing velocity models to locate the events. Travel times to distant stations (stations 15 and 16), however, provide additional data for determination of lunar structure to a depth of about 120 km.

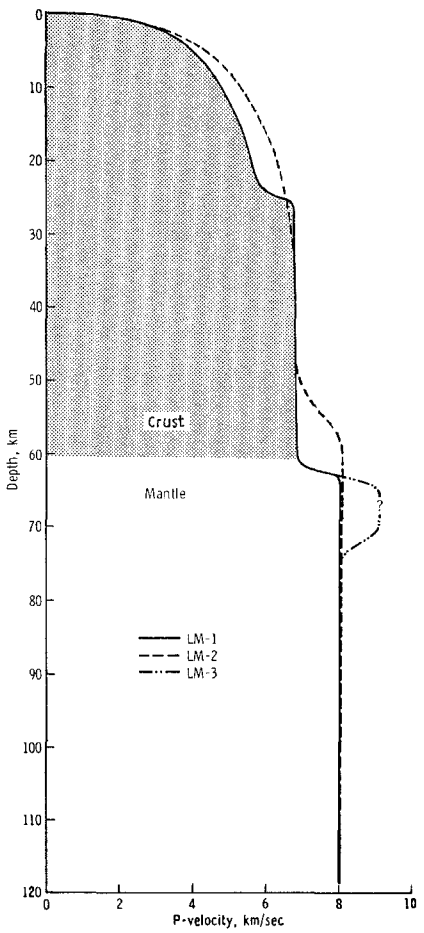

Fig. 7. Compressional velocity models based on different data subsets. Dashed curve (LM-2) fits the travel times and first arrival amplitudes. The solid curve (LM-1) fits above data and is further modified on the basis of synthetic seismograms. Model LM-3 shows the possible high-velocity layer beneath the crust based on unreversed profile.

Interpretation of the seismic data is based upon calculations of theoretical seismic wave amplitudes and travel times for assumed lunar models. Model parameters are adjusted until the theoretical results are brought into satisfactory agreement with the observed travel-time and amplitude data. Theoretical seismograms have been computed for 'best fitting' models. Detailed comparison of the wave forms of the theoretical and experimental seismograms provides a further check on the adequacy of the model. A model that fits the travel-time and amplitude data for P-waves, designated LM-2 (Lunar Model 2) is shown in Figure 7. A second model, LM-1, assumes that later arrivals are correctly interpreted as P waves reflected at the surface and from horizons at depth. This interpretation introduces a discontinuity at 25 km and sharpens

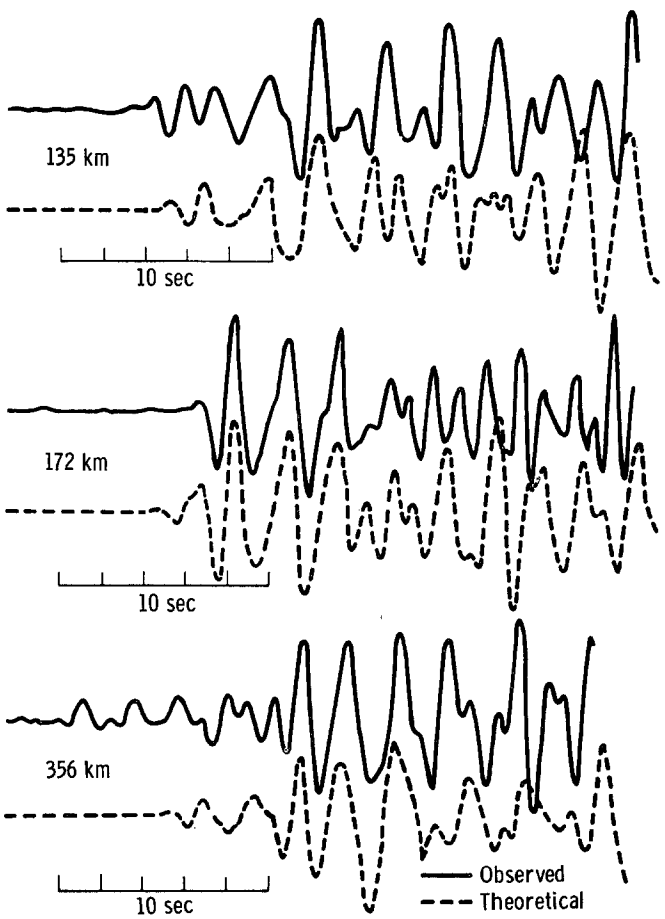

Fig. 8. Observed (solid line) and synthetic P-wave seismograms for three S-IVB impacts recorded at station 12. Seismogram character and relative amplitudes of first and later arrivals change with distance. The source function used in the calculation of the theoretical seismograms was selected by requiring a close match with the first 10 s of the seismogram recorded at a range of 172 km. At 356 km, the first two peaks of the observed seismogram are filtered noise pulses. Theoretical seismograms for $\Delta = 132$ and $\Delta = 243$ km (not shown) also fit the observed records.

the velocity change at about 60 km. Confidence in this interpretation is strengthened by the close match between theoretical seismograms based upon this model and the observed data, shown in Figure 8. However, in the presence of intensive scattering, interpretation of secondary arrivals cannot be made with high confidence. Thus, the discontinuity at 25 km in model LM-1 should be regarded as tentative pending receipt of corroborative data. Model LM-3 is the same as LM-1 except that a thin, high-velocity layer is introduced just beneath the main discontinuity at 63 km. The presence of the high velocity layer is supported by only one data point: A small pulse at the beginning of the wavetrain detected at station 12 from the Apollo 15 S-IVB impact. If such a layer does exist, its thickness must be less than about 20 km. It may be confined to the region of the Apollo 12 and 14 stations. Other explanations for the early pulse that would invalidate the interpretation are possible. For example, the occurrence of an ill-timed noise pulse, or a steeply dipping, refracting horizon could also account for a high apparent velocity. Thus, the existence of the high velocity layer must be regarded as tentative pending further supportive evidence. Features common to all of the models are the following:

(1) Velocities increase very rapidly to a depth of about 10 km. Very low velocities near the surface correspond to those of the lunar soil and broken rocks representing the regolith. The rapid increase of velocity can be explained by progressive compaction.

(2) The velocity of seismic waves (compressional) is about 7 km s^{-1} throughout the deeper half of the mare crust. Among the major lunar rock types identified thus far, this velocity is close to that expected for only one type – the gabbroic anorthosites – which predominate in the highlands of the Descartes site.

(3) An abrupt increase in compressional velocity, to 8.1 km, occurs at a depth of about 60 km. By analogy with the Earth, the material above this discontinuity is referred to as the crust; and the material below is called the mantle. The upper mantle velocity of 8.1 km s^{-1} corresponds to that of terrestrial olivines, pyroxenites, and peridotites and is consistent with the petrological inferences made from the analysis of lunar samples [15, 16, 17, 18].

2. *The Deep Lunar Interior*

Seismic data relevant to the structure and state of the deep lunar interior derive from deep moonquakes and from distant impacts. The presence or absence of shear waves, which cannot propagate through a liquid, and the travel times of both compressional waves (P) and shear waves (S) from these events are the most direct sources of information.

High frequency shear waves (0.5 Hz and higher) have been detected from all moonquakes with epicenters on the near side of the Moon located thus far. Thus, since these signals originate at depths approaching 1000 km, we can say immediately that widespread melting cannot occur in the outer 1000 km of the near-side portion of the Moon. The locations of moonquake foci are based upon a seismic velocity model derived by extrapolation of upper mantle velocities, determined from the LM and S-IVB impacts, to great depth. In the two cases (Moonquake foci A_{15} and A_{20}) for

which redundant data are available (P at one station and S at all four stations), the validity of this extrapolation can be checked. In both cases, the observed travel times agree within a few seconds with those predicted from the model. Thus, it appears that the compressional wave velocity must remain within a few percent of 8 km s^{-1} to a depth of nearly 1000 km. A slight decrease in velocity with depth, or increase in Poisson's ratio, is suggested by the available data.

Several events that originated on the far side of the Moon have recently been discovered: a meteoroid that struck near the crater Moscoviense on July 17, 1972; and two moonquakes from an active zone (A_{33}) for which the preliminary epicentral location is 139° E, 7° S. Shear waves from these events cannot be identified in the records at several of the stations. The missing shear waves and the observed P-wave travel times can be explained by introducing a molten, or partially molten core, or shell, within the moon beginning at a depth of about 1000 km, i.e., just beneath the moonquake zone. Completely solid lunar models, for which shear waves would not be observed over certain distance intervals (the 'shadow-zone'), are possible. However, it is difficult to conceive of a model of this type that will adequately explain the data from both the deep seismic source (A_{33} moonquake) and the surface source (July 17 impact).

A high-density (metallic) core of the size suggested by our preliminary analysis is ruled out by moment-of-inertia considerations [25]. Thus, the most plausible hypothesis that can be advanced at present is that we are dealing with a silicate interior in which the solidus temperature is exceeded at a depth of about 1000 km. The model proposed here is in substantial agreement with several thermal models recently proposed by Toksőz *et al.* [14]. By analogy with the Earth, it begins to appear that we may consider the lunar lithosphere – the relatively rigid outer shell of the Moon – to be about 1000 km thick.

C. MOONQUAKES AND LUNAR TECTONISM

1. *Observational Data*

Hundreds of moonquakes were recorded at station 16 during the initial 45-day period of operation. From this sample, it is estimated that approximately 10000 moonquakes per year will be detected by the Descartes station. By comparison, moonquakes are recorded at station 14 at a rate of about 2000 per year; and at stations 12 and 15 at a rate of 700 per year. Thus, we can expect to record about 700 moonquakes simultaneously at all four seismic stations each year. Fewer than 25% (about 180) will be large enough to permit detailed analysis of their waveforms. Variations in the rates of moonquake detection among the stations is believed to be a consequence, primarily, of differences in the local regolith thickness of each site. Corresponding variations in the amplification of ground motion would account for the differences in station sensitivity. That the station sensitivities do vary is confirmed by relative amplitude measurements for seismic signals from the S-IVB impacts.

All of the moonquakes are small. With one possible exception, the largest of them

have Richter magnitudes of between 1 and 2, and most moonquakes are much smaller than this. The total seismic energy release within the Moon appears to be many orders of magnitude below that of the Earth.

As described in earlier papers [4–12], signals from moonquakes are distinguished from those of meteoroid impacts primarily by the relative prominence of the shear wave (originally called the H-phase) and differences in the signal rise times (the time interval between the beginning of a wavetrain and its peak amplitude). The shear wave is much more prominent in the wavetrains from moonquakes than in those from meteoroid impacts, and the rise times of moonquake signals are characteristically much shorter than those of meteoroid impact signals.

With few exceptions, the signals from all moonquakes, large enough to permit detailed analysis of their waveforms, can be grouped into sets: members of each set having waveforms which match one another in detail. Events within each group of matching signals occur at regular intervals, normally once per month, and at specific times during the lunar orbit. In some cases, as many as 3 or 4 events of a given matching group will occur during a monthly cycle, but such multiple events occur over a relatively short interval of five days, or less. The repetitious character of these events strongly supports the hypothesis that they are moonquakes; each group of matching signals corresponding to an active zone or focus within the Moon at which repeating moonquakes originate. The monthly periodicities suggest that rupture is induced by tidal stresses.

With the aid of the fourth seismic station (station 16), 33 categories of matching events have been identified. Thus, there must be at least 33 zones within the Moon at which the repeating moonquakes originate. Many additional active zones, from which the signals are too small to permit detailed analysis of their waveforms, probably exist.

TABLE I

Moonquake locations and number of moonquakes identified in each category

Moonquake category	Latitude	Longitude	Depth, km	Number[c] identified
A_1	23.3° S	28.3° W	850	64
A_6[a]	23.3° S	28.3° W	850	19
A_7	15.0 N	25.0° E	700[b]	21
A_{14}	44.8° S	53.4° W	800[b]	15
A_{15}	9.2° N	8.4° W	610	3
A_{18}	30.2° N	2.9° E	800	14
A_{20}	22.3° N	30.2° W	940	2
A_{25}	22.8° N	61.1° E	860	7
A_{33}	7° S	139° E	800[b]	2

[a] A_6 focal zone is within about 20 km of the A_1 focal zone.

[b] Data are not sufficient for determination of focal depth. The listed focal depths were assumed in the calculation of epicentral coordinates.

[c] A total of 319 moonquakes have been identified to date (September, 1972) from all 33 active moonquake zones.

Thus far, signals from six of the moonquake foci have been large enough to provide data necessary to compute the source location. Epicentral locations can be determined in three additional cases if focal depths are assumed. The solutions obtained are listed in Table I. The moonquake epicenters (point on the surface immediately above the focus) are plotted in Figure 9. Seismograms for a moonquake recorded at all 4

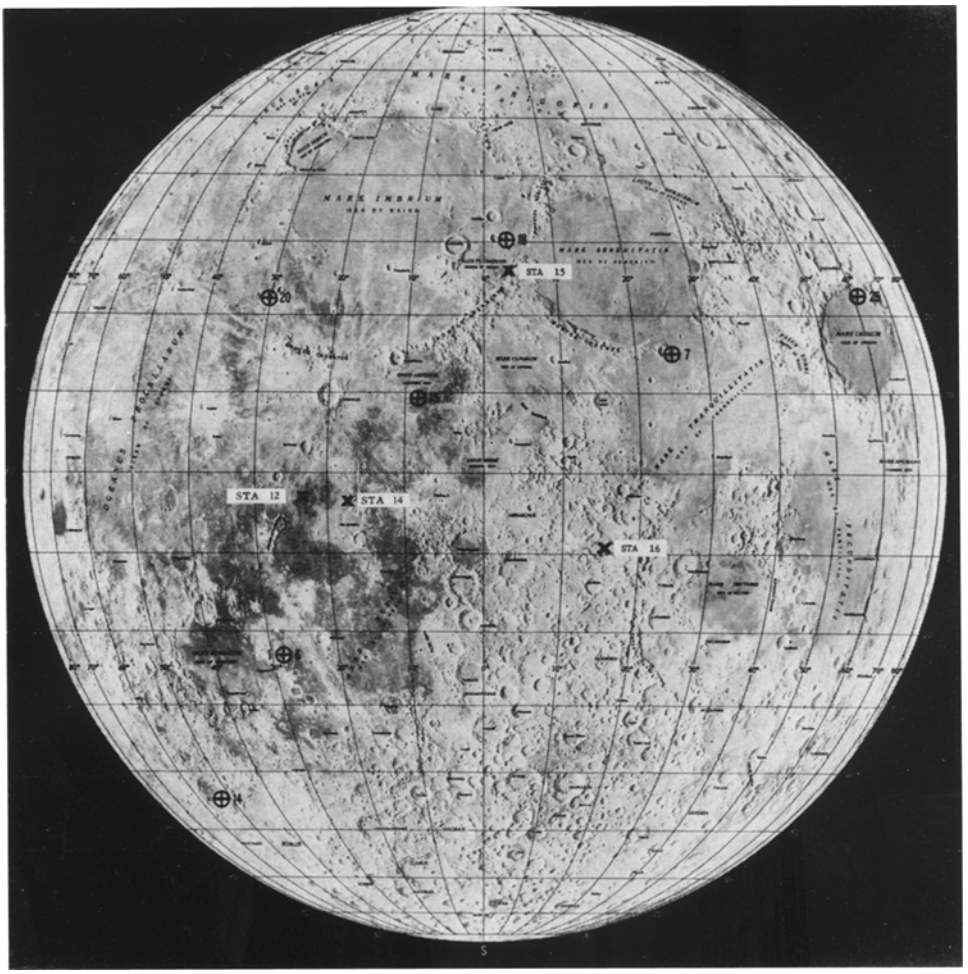

Fig. 9. Map showing the locations of the Apollo 12, 14, 15, and 16 seismic stations and the category A moonquake epicenters. Station numbers indicate the Apollo missions in which the stations were installed. Numbers at moonquake epicenter markers identify the epicenters listed in Table I.

stations are shown in Figure 10. All of the focal depths determined thus far, fall between 600 km and 940 km.

2. *The Influence of Tides*

As noted above, moonquakes from each active zone occur at monthly intervals.

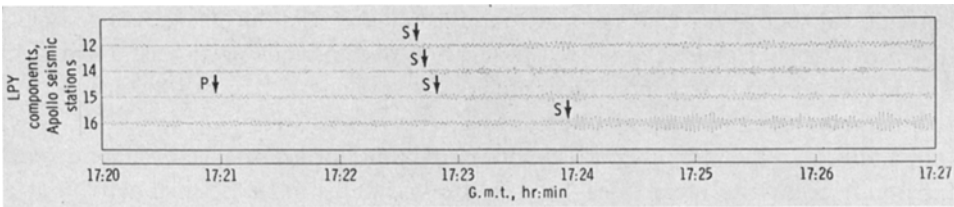

Fig. 10. Records of a category A_{20} moonquake detected at the Apollo 12, 14, 15, and 16 sites on May 15, 1972. The LPY component seismograms are shown for each station. The most prominent phases are interpreted as the direct compressional wave (P-wave) and the direct shear wave (S-wave) arrivals. A moonquake focus can be uniquely located on the basis of four P- and/or S-wave arrival times at three or more seismic stations given a seismic velocity model for the lunar interior. Using the S-wave arrival times at the four stations, the category A_{20} moonquake focus is located at 22.3° N and 30.2° W at a depth of 940 km.

Peaks in total moonquake activity, taken as the summation of all events detected at a given station per unit time, occur at intervals of about 14 days. This periodicity is shown in Figure 11, where the number of moonquakes per day detected at station 12

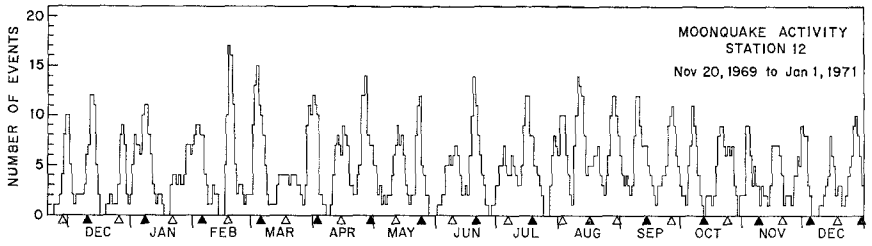

Fig. 11. Number of moonquakes per day recorded at station 12 for the period November 20, 1969, to January 1, 1971, plotted as a three-day running sum, a total of 650 events are plotted. Solid triangles indicate times of perigee; open triangles indicate apogee.

during 13 months of operation has been plotted. The most prominent peaks in the spectrum computed for the activity plot of Figure 11 occur at periods of 14 and 28 days. These are the periods of the principal tidal components. The same periodicity is observed for moonquakes detected at stations 14, 15, and 16. In general, peaks in moonquake activity occur near times of apogee and perigee. However, the pattern of moonquake occurrence is not related simply to the monthly changes in earth-moon separation (the apogee perigee cycle), but is complicated by other tidal components arising from the lunar librations and solar perturbations of the lunar orbit. We defer further discussion of the tidal influence in moonquake occurrence until correlative data are better determined. However, it seems safe to conclude that tidal stresses play a major role in the seismicity of the Moon.

3. *The Focal Mechanism*

Although the exact nature of moonquake focal mechanisms is presently unknown, some statements can be made. The nearly exact repetition of moonquake signals from

a given focal zone over periods of many months requires that the focal zones be small, 10 km in diameter or less, and fixed in location over periods of at least 2 years. If moonquake foci were separated by as much as 1 wavelength, larger differences would be observed among moonquake signals.

In addition to the monthly periodicities in the times of occurrence of moonquakes apparently related to lunar tides, longer-term variations in the seismic activity at a given focus can also be correlated with tidal variations [8]. Hence, tidal strain must contribute significantly to the total strain energy released as moonquakes. Tidal energy may, in fact, be the dominant source. However, the unipolarity of moonquake signals from a given focal zone implies that the source mechanism is a progressive dislocation and not one that periodically reverses in direction. A progressive source mechanism suggests a secular accumulation of strain energy periodically released by moonquakes. Whether the postulated secular strain component is of thermal or gravitational origin remains to be determined.

As described above, moonquakes appear to be concentrated at great depth. In the few cases for which locations have been determined, the foci occur in a zone between 600 km and 940 km deep. Of course, many of the foci not yet located, may fall outside this zone.

Moonquake epicenters located thus far coincide closely with the rims of the major mascon basins. The significance of such a correlation, must be questioned carefully pending the proposal of a reasonable mechanism by which a narrow feature, such as a mare rim, could show any manifestation at such great depth, and only in a narrow range of depths.

The newly discovered evidence suggesting the presence of a molten, or partially molten, zone at great depth, if confirmed, will have an important bearing on the question of the focal mechanism of moonquakes. The localization of moonquake activity in a zone 400 km thick, falling immediately above the zone of melting, may then be explained as resulting from one or more of the following factors: (1) fluids injected into the moonquake zone from below, under the influence of tides, would lead to a reduction of effective friction along zones of weakness, or weakening of the silicate bond, leading to dislocation; (2) reduced rigidity in the zone of melting would tend to concentrate the dissipation of tidal energy at great depth; (3) maximum thermoelastic stresses would be expected in the region bounding the zone of melting; and (4) weak convective motions beneath a thick, rigid mantle might generate deep moonquakes without the surface manifestations associated with terrestrial plate tectonics.

D. METEOROID FLUX

Many of the signals detected by the Apollo seismic network are generated by meteoroid impacts. These are distinguished from moonquake signals primarily because of their similarity to signal waveforms generated by the LM and S-IVB impacts. The latter also serve to calibrate the relationship between signal energy and kinetic energy of the impacting body. Owing to the limited quantity of multi-station data available thus far, a statistical method requiring data from a single station only, has been

employed. The present discussion will be limited to a brief outline of the method and summary of results. The interested reader is referred to Latham *et al* [24] for details. More accurate estimates of meteoroid flux, using multi-station data for location of each impact, will be made as soon as sufficient data accumulate.

Earth-based observations have previously produced estimates of the meteoroid population in terms of the parameters B and λ (arbitrary constants) in the distribution

$$\log N = B + \lambda \log m\,, \tag{1}$$

where N is the count of particles/km^2/yr with mass m grams or greater which hit the Earth. Notably, Hawkins [20] found $B=-0.73$, $\lambda=-1.0$ for stony meteoroids (masses about 300 gm to 10^{10} gm) by compiling visual data on falls and finds, while McCroskey [22] has obtained $B=-1.6$, $\lambda=-0.62$ from photographic measurements of luminous meteoroid trails observed by the Prairie network. Our objective is to measure B and λ independently by means of lunar seismic data.

McCrosky obtained direct photographic velocity measurements for individual bodies by means of shutter breaks. His analysis is consistent with a preatmospheric average velocity of 25 km s^{-1} for the population. For lunar impacts, this would be equivalent to 22.5 km s^{-1} because of weaker gravitational acceleration near the Moon. We estimate that for this impact velocity, the minimum detectable seismic signal is produced by less than 100 g at a distance of 50 km from the seismic station and about 10 kg at the antipodal point of the Moon. The largest signals yet observed were produced by an object falling about 221 km from station 12 on May 13, 1972, shortly after deployment of station 16. At 22.5 km s^{-1}, a mass of about 1100 kg would have produced the signal observed at this range. Since only a few of the strongest natural impacts have been located from their seismic signals, other objects of similar size may be represented by weaker signals from greater distances. Thus, the objects observed by seismic impact signals appear to be in the lower part of the mass range dominated according to Hawkins [20], by stony meteoroids.

The basic data from the seismic experiment can be represented as a cumulative count, n (per year), of events whose signal amplitudes are equal to or greater than A (mm) on the seismic trace. Impact signals observed during 399 days at station 12, as represented in Figure 12, were used in the present analysis. In this sample interval, all events with maximum peak-to-peak envelope amplitudes greater than about 2.5 mm were examined and classified as either spurious instrumental deflections, moonquakes or meteoriod impacts on the basis of signal character. Only the latter were included among the 64 events used here. The ranges and masses of individual impacts in this distribution are unknown, but the intercept and slope of the linear distribution as indicated by the equation in figure 12, are used in evaluating the B and λ values of the meteoroid distribution corresponding to the seismic signals.

An essential element, the amplitude responce of the Moon to an impact of standard size as a function of range, is available from the impacts of the S-IVB booster vehicles as observed at the various stations. These amplitude data are plotted in Figure 13. Here, the primary artificial impact amplitude measurements are made on the LPZ

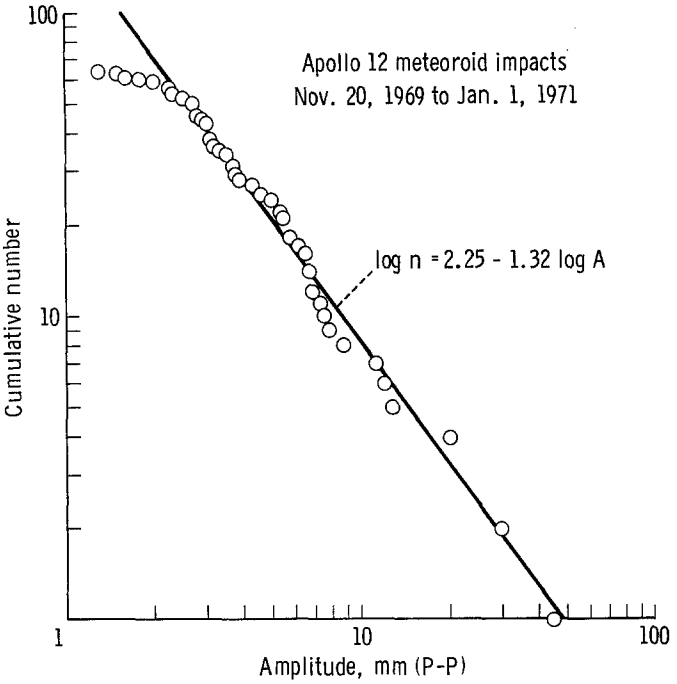

Fig. 12. Cumulative amplitude distribution for 64 meteoroid impact events. The ordinate of each point represents the number of events observed to have signals of amplitudes equal to or greater than represented by the abscissa of the point. After subtracting instrument downtime, the net interval of observation is 399 days between November 20, 1969, and January 1, 1971. The amplitudes measured are the maximum peak-to-peak amplitudes (mm) of the signal envelope recorded on the LPZ component at station 12, with trace deflection 0.8 mm per digital unit. For analysis, the data are represented by the straight line shown. Its equation after conversion to an annual rate is $\log n = 2.16 - -1.32 \log A$, A in mm, n in events observed per year.

component of station 12. Data of other stations, which are more sensitive than station 12 due to effects of shallow layering, have been adjusted to represent peak-to-peak envelope amplitudes which would have been recorded by station 12 at the same range. The station corrections are made by comparing the amplitudes of signals recorded at two or more stations from a representative sampling of natural events. Extensions of the curve of Figure 13 outside the range interval for which data are available are based upon theoretical calculations; assuming two-dimensional diffusive spreading at near ranges and conventional geometric ray spreading at far ranges.

An important constraint arises from the distribution of crater sizes observed on the lunar surface. For the present analysis, we have used the measurements quoted by Gault [21] for the youngest mare surface examined (south-eastern Oceanus Procellarum). Hence, the crater diameter distribution is of the form $N \propto d^{-3.7}$ for diameters from 100 m to 1000 m, where N is the number of craters per unit area and d is crater diameter. Combining this with a meteoroid mass (m) vs diameter scaling law in the range $m \propto \mathrm{d}^{3.0}$ to $m \propto d^{3.4}$, as suggested by Gault, the corresponding range of values

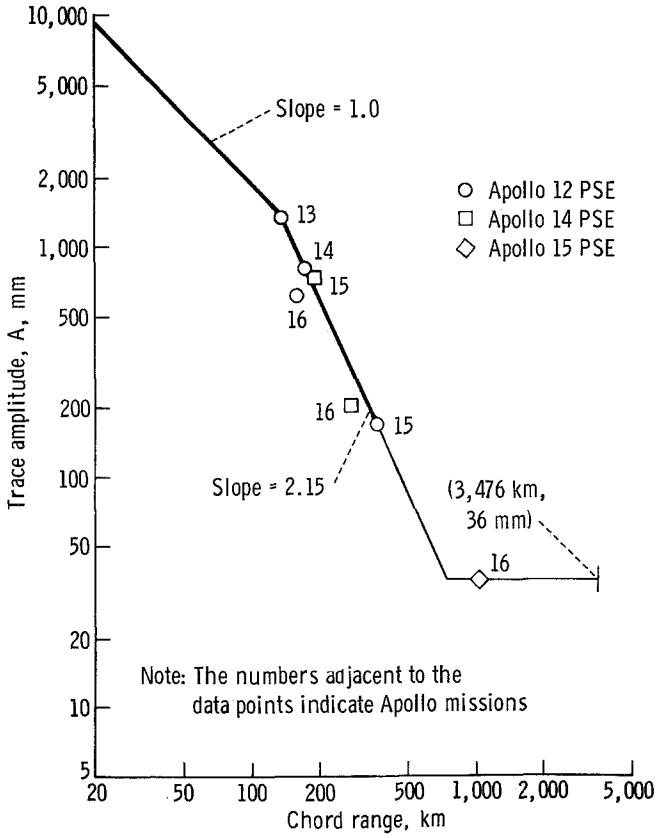

Fig. 13. Amplitude variations with range for S-IVB impacts recorded on the LPZ components. The open circles represent measurements of the Apollo 12 LPZ component. Other symbols are data derived from recordings at other stations. The number written beside each symbol identifies the mission during which that datum was obtained. All amplitudes except the Apollo 12 LPZ data are scaled for station sensitivity as described in the text. The amplitudes were measured as maximum peak-to-peak deflections of 90% of the swings at the time of maximum signal envelope on Brush oscillograph playouts at a chart speed of 3.75 mm min^{-1}. Amplitudes plotted represent a deflection sensitivity of about 0.8 mm/digital unit (exactly 20×4 cm/1023 D.U.). Most records were measured at lower deflection sensitivities and scaled accordingly.

for the parameter λ in equation 1 is $-1.23 < \lambda < -1.09$. Hawkins' value of λ falls slightly outside this range, while McCrosky's is quite far from it.

Therefore, in order to calculate the mass flux of meteoroids we accept: (1) the lunar seismic flux at station 12 as shown in Figure 12 and represented by $\log n = 2.16 - 1.32 \log A$ per year; (2) the seismic sensitivity of the Moon as represented by the response of station 12 LPZ to S-IVB impacts at all ranges, given by the curve of Figure 13; (3) the average impact velocity of 22.5 km s^{-1} derived from McCrosky's Earth-based observations of luminous meteoroid trails; (4) the constraint $-1.23 \leqslant \lambda \leqslant -1.09$ derived from the size distribution and scaling relationships for crater diameters. All of these except item 3 are derived from measurements on the Moon. With these data, two new lunar flux models are calculated by methods described by Latham

et al. [24]. In Figure 14, these new results are compared with McCrosky's and Hawkins' Earth flux models. The two lunar curves correspond to the limits, $\lambda = -1.23$ and $\lambda = -1.09$, based on Gault's discussion.

The difference between the two lunar flux models is minor compared with their

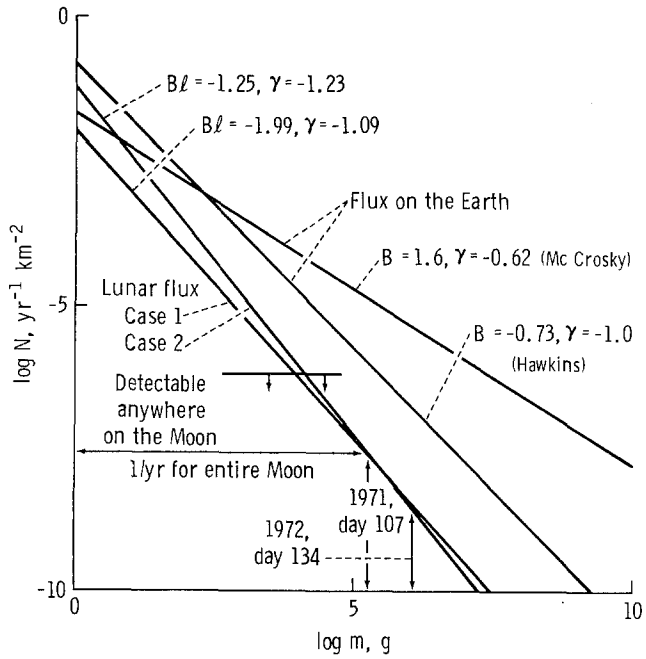

Fig. 14. Lunar flux curves representing a range of likely values (Cases 1 and 2) from lunar data are compared with earlier flux measurements from Earth by Hawkins and McCrosky. An impact velocity of 22.5 km s^{-1} is implicit in the lunar curves. At this velocity, direct comparison of Earth and lunar flux requires that the lunar curves should be raised by 0.09 units on the y-axis to correct for earth vs lunar gravitational focussing. For the lunar surface area of 3.794×10^7 km^2 the level of one event per year is represented at -7.58 on the log frequency scale as shown. Mass values for two large events not included in the interval of the data sample are indicated: 1971 day 107 had moonquake waveform characteristics but fits the impact statistics much better than the moonquake statistics; 1972 day 134 had an impact waveform and was the strongest signal ever observed. The smallest mass detectable from any point on the Moon is slightly different for Cases 1 and 2 because the different values for 2β for these cases imply a difference in seismic coupling for impacts of the same mass.

great departure from the previously measured Earth flux models. Several possible explanations can be discussed. There may be strong secular variations in the flux. The intervals of observation do not overlap, but only about 3 years elapsed from the end of McCrosky's observations until the start of ours. While annual fluctuations are to be expected if particle orbits cluster into streams, both McCrosky's data and ours span an interval of more than one year (500 days and 399 days, respectively) which should greatly reduce such effects.

In the lunar seismic analysis further data on seismic coupling efficiency at various

masses, energies, and velocities would be desirable. The energy of the calibration impacts, S-IVB's striking at about 2.56 km s^{-1}, is about the same as that of a 180 kg meteoroid at 22.5 km s^{-1}. This seems to be near the upper end of the range of observed natural masses, but not outside the range. However, for signal calibration purposes we have not included data from LM impacts because their very low velocities (about 1.7 km s^{-1}) and grazing angles (about 3° from the horizontal) probably make these events very different from natural impacts.

The statistics of our models of lunar flux predicts an average rate of occurrence for impacts as large as that of May 13, 1972, of only 1 per ten years for the entire Moon. However, the mass of the recently discovered impact of July 17, 1972, is comparable to that of the May 13 impact. The occurrence, of two events of such predicted rarity within three months, suggests that our present flux estimate must be applied with caution pending analysis of data from a longer period of time. The ability to estimate the locations of natural impacts, which has been acquired with the deployment of station 16, clearly suggests new methods of analysis for data recorded after April 1972. Locating, roughly at least, many of the larger impacts will permit a more direct measurement of the areal density of detectable impacts, particularly since the minimum detectable mass appears to be constant for ranges beyond about 700 km from a station (see below). The latter result itself can be tested by simultaneous four-station observations.

The various flux estimates represented by Figure 14 have interesting implications regarding the history of the Moon and the solar system. Wetherill [23] has noted the difficulty of reconciling the high previous measurements of flux with the relatively low present crater density and the great ages of the lunar maria which have been established during the Apollo program. He refers to flux too high by a factor of 35 by comparison with the mare crater densities quoted by Gault. It is true that the masses observed on the lunar seismograph network fall a little short of the size range that produces craters visible in the Lunar Orbiter photos. However, if we extrapolate our mass flux curve out to 10^6 kgm, about 3 or 4 orders of magnitude beyond our data, we see that it indicates an abundance about 2 orders of magnitude less than Hawkins's estimate and more than 4 orders of magnitude less than McCrosky's. This would represent a lower present flux rate than the average needed to produce the visible mare craters in 3.5×10^9 yr. This result is consistent with the concept of a secular decrease of flux as smaller fragments in the solar system are swept up by the planets. Clearly, all methods of meteoroid flux estimation must be critically examined until the large discrepancies among present results are understood.

4. Summary and Conclusions

(1) Analysis of seismic data from man-made impacts have established the presence of a lunar crust approximately 60 km thick in the region of stations 12 and 14. The velocity of seismic waves (compressional) is about 7 km s^{-1} throughout the deeper half of the mare crust. Among the major lunar rock types identified thus far, this velocity is close

to that expected for only one type–the gabbroic anorthosites–which predominate in the highlands of the Descartes site. Results from the X-ray fluorescence experiment, carried out from lunar orbit, suggest that this rock type is representative of the lunar highlands on a global scale. Thus, combining in situ velocity information with laboratory data from returned lunar samples, the most probable hypothesis that can be put forward at present is: (a) The primitive lunar crust, which outcrops in the highlands, is approximately 60 km thick in the region of the Apollo seismic network; (b) It consists primarily of gabbroic and anorthositic material; (c) The maria were formed by the excavation of the initial crust by meteoroid impacts and subsequent flooding by basaltic material; (d) Seismic evidence suggests that the basalt layer may be 25 km thick in the southeastern portion of Oceanus Procellarum; comparable to the thickness inferred for mascon maria.

(2) Beneath the base of the crust, the velocity of compressional waves increases abruptly to about 8.1 km s^{-1} and remains close to this value to a depth of about 1000 km. By analogy with the Earth, this zone is referred to as the mantle. In fact, the compressional-wave velocity of 8.1 km s^{-1} determined for the upper mantle of the Moon is very close to the average for rocks of the upper mantle of the Earth. Signals from the man-made impacts and deep moonquakes show that the elasticity of the upper mantle is appropriate for rocks of high rigidity (Poisson's ratio $=0.25$) and that no widespread zone of melting or partial melting can exist in the outer 1000 km of the Moon. If the lunar crust were derived by differentiation, as seems probable, then widespread melting of the outer shell of the Moon early in its history is inferred from the thickness of the lunar crust. The required depth of melting depends upon the assumed initial composition of the Moon, but it is likely that at least 50% of the Moon was differentiated early in its history.

(3) Preliminary analysis of recently acquired seismic data from lunar farside events (one meteoroid impact and two moonquakes) suggests that melting begins within the present-day Moon at a depth of about 1000 km. The velocity of compressional waves is lower in the zone of melting than it is within the mantle above, but the velocity change required to fit the data is small. Melting alone may be sufficient to explain the velocity contrast; although, an associated change in composition, or phase, cannot be ruled out at present.

(4) Moonquakes are recorded at all Apollo seismic stations. Based upon the data obtained during the first 45 days of operation of station 16, moonquakes are detected at this station at an average rate of about 10000 per year. This compares with the annual rates of 650, 2000, and 750 at stations 12, 14, and 15, respectively. The varying rates of detection are believed to be a consequence primarily of differing station sensitivities which appear to be closely correlated with the local structure and the thickness of the weakly cohesive material of the surficial zone at each site. All of the moonquakes are small. With one possible exception, the largest of them have equivalent Richter magnitudes between 1 and 2. The total seismic energy release within the Moon appears to be many orders of magnitude below that of the Earth.

(5) The recognized categories of moonquake signals now number 33. We infer that

moonquakes originate at no less than 33 different locations, and that moonquakes originate at numerous other active zones from most of which the signals are too weak to be analyzed in detail with the existing seismograph network. Each focal zone must be small (less than 10 km in linear dimension) and fixed in location for periods of at least two years. Moonquakes also show a monthly periodicity in their times of occurrence. Peaks in the total number of events detected at a given station occur at approximately 14-day intervals. These cycles strongly suggest that moonquakes are induced by lunar tides. However, the pattern of moonquake occurrence is not related simply to the monthly changes in earth-moon separation (the apogee – perigee cycle), but is complicated by the influence of lunar librations and solar perturbations of the lunar orbit.

(6) All of the active zones for which depths have been determined (six cases), occur in the depth range from 600 to 1000 km. On Earth, deep quakes are associated with lithospheric slabs which sink to great depth in a global convection system. On the Moon, where all evidence appears to preclude the presence of such plate movements, other explanations for deep quakes must be sought. If, as preliminary evidence suggests, a zone of melting presently exists within the moon beginning at a depth of about 1000 km, it undoubtedly plays a major role in the generation of deep moonquakes. Several possible mechanisms are: (a) Maximum thermoelastic stresses in a cooling Moon occur at depths of 600 to 1000 km; (b) Abrupt phase changes of mantle material are occurring in the active focal zones; (c) A concentration of fluids at great depth leads to a reduction of effective friction or a weakening of the silicate bond; (d) Weak convective motions at depth beneath a thick, rigid mantle might generate deep moonquakes without the surface manifestations associated with terrestrial plate tectonics; (e) Radial variations in rigidity of the lunar material may be such as to concentrate the dissipation of tidal energy at great depth.

(7) The distribution of moonquake epicenters (point on the lunar surface directly above the focus) shows an apparent correlation with the rims of the major mascon basins. The significance of this pattern must be questioned pending the proposal of a reasonable mechanism by which a narrow surface feature, such as a mare rim, could influence activity at such great depth, and in a narrow range of depths only.

(8) Seismic signals from meteoroid impacts appear to be generated by objects in the mass range 100 gm to 1000 kg. The specific flux estimated from the accumulated data varies from 1 to 3 orders of magnitude lower than that derived from photographic measurements of the luminous trails of meteoroids striking the atmosphere of the Earth. Our mass flux estimate is also lower than the average flux estimated from the distribution of crater sizes on the youngest lunar maria. This is consistent with a hypothesis that the population of small fragments in the solar system decreases with time as they are gathered up by collisions with the planets. The seismic data predict that between 30 and 40 impacts per year will be detected simultaneously by all stations of the Apollo seismic network, and that a meteoroid of mass 7 to 10 kg can be detected by the least sensitive station (station 12) from any point on the Moon. The average of acceptable flux estimates derived from seismic measurements is

$$\log N = -1.62 - 1.16 \log m,$$

where N is the cumulative number of meteoroids of mass m (in g) and greater, which strike the Moon per year per km^2.

(9) The surface of the Moon is covered by a highly heterogeneous layer in which seismic waves propagate with relatively little damping but are intensively scattered. It is the presence of this layer (the 'scattering zone') that accounts for the marked differences between lunar seismic signals and typical terrestrial seismic signals. Most of the heterogeneity effective in scattering seismic waves at the observed frequencies is confined to the upper several hundred meters of the surface layer; although the total thickness of the zone in which significant scattering occurs may be as great as 10 to 20 km. It is probable that the complex structure of the surface layer of the Moon is a consequence primarily of cratering processes.

References

[1] Latham, G., Ewing, M., Press, F., Sutton, G., Dorman, J., Nakamura, Y., Toksőz, N., Wiggens, R., Derr, J., and Duennebier, F.: 1969, 'Passive Seismic Experiment', Sec. 6 of Apollo 11 Preliminary Science Report, NASA SP-214.

[2] Latham, G., Ewing, M., Press, F., Sutton, G., Dorman, J., Nakamura, Y., Toksőz, N., Wiggens, R., Derr, J., and Duennebier, F.: 1970a, *Science* **167**, 455–467.

[3] Latham, G., Ewing, M., Press, F., Sutton, G., Dorman, J., Nakamura, Y., Toksőz, N., Wiggens, R., Derr, J., and Duennebier, F.: 1970b, *Geochim. Cosmochim. Acta Suppl.* **1**, 2309–2320.

[4] Latham, G., Ewing, M., Press, F., Sutton, G., Dorman, J., Nakamura, Y., Toksőz, N., Wiggens, R., and Kovach, R.: 1970c, 'Passive Seismic Experiment', Sec. 3 of Apollo 12 Preliminary Science Report, NASA SP-235.

[5] Latham, G., Ewing, M., Press, F., Sutton, G., Dorman, J., Nakamura, Y., Toksőz, N., Meissner, R., Duennebier, F., and Kovach, R.: 1970d, *Science* **170**, 620–626.

[6] Ewing, M., Latham, G., Press, F., Sutton, G., Dorman, J., Nakamura, Y., Meissner, R., Duennebier, F., and Kovach, R., 1971, in *Highlights of Astronomy*, D. Reidel Publ. Co., Dordrecht, Holland, pp. 155–172.

[7] Latham, G., Ewing, M., Press, F., Sutton, G., Dorman, J., Nakamura, Y., Toksőz, N., Duennebier, F., and Lammlein, D.: 1971, 'Passive Seismic Experiment', Sec. 6 of Apollo 14 Preliminary Science Report, NASA SP-272.

[8] Latham, G., Ewing, M., Press, F., Sutton, G., Dorman, J., Nakamura, Y., Lammlein, D., Duennebier, F., and Toksőz, N.: 1971, *Science* **174**, 687–692.

[9] Latham, G., Ewing, M., Press, F., Sutton, G., Dorman, J., Nakamura, Y., Toksőz, N., Lammlein, D., and Duennebier, F.: 1972, 'Passive Seismic Experiment', Sec. 8 of Apollo 15 Preliminary Science Report, NASA SP-289.

]10] Latham, G., Ewing, M., Press, F., Sutton, G., Dorman, J., Nakamura, Y., Toksőz, N., Lammlein, D., and Duennebier, F.: 1972, *Proceedings of the Third Lunar Science Conference, Geochim. Cosmochim. Acta Suppl. 3*, **3**, M.I.T. Press.

[11] Latham, G., Ewing, M., Press, F., Sutton, G., Dorman, J., Nakamura, Y., Toksőz, N., Lammlein, D., and Duennebier, F.: 1972, *The Moon* **4**, 373–382.

[12] Toksőz, N., Press, F., Dainty, A., Anderson, K., Latham, G., Ewing, M., Dorman, J., Lammlein, D., Sutton, G., and Duennebier, F.: 1972, *Proceedings of the Third Lunar Science Conference, Geochim. Cosmochim. Acta Suppl. 3*, **3**, M.I.T. Press.

[13] Toksőz, N., Press, F., Dainty, A., Anderson, K., Latham, G., Ewing, M., Dorman, J., Lammlein, D., Sutton, G., Duennebier, F., and Nakamura, Y.: 1972, *The Moon* **4**, 490–504.

[14] Toksőz, N., Solomon, S., Minear, J., and Johnston, D.: 1972, *The Moon* **4**, 190–213.

[15] Ringwood, A. and Essene, E.: 1970, *Proceedings of the Apollo 11 Lunar Science Conference, Geochim. Cosmochim. Acta Suppl. 1*, **1**, Pergamon Press, New York, pp. 769–799.

[16] Smith, J., Anderson, A., Newton, R., Olsen, E., Wyllie, P., Crewe, A., Isaacson, M., and

Johnson, D.: 1970, *Proceedings of the Apollo 11 Lunar Science Conference, Geochim. Cosmochim. Acat Suppl. 1*, **1**, Pergamon Press, New York, pp. 897–925.
[17] Green, D., Ringwood, A., Hibberson, W., Major, A., and Kiss, E.: 1971, *Proceedings of the Second Lunar Science Conference, Geochim. Cosmochim. Acta Suppl. 2*, **1**, M.I.T. Press, pp. 601–615.
[18] Biggar, G., O'Hara, M., Peckett, A., and Humphries, D.: 1971, *Proceedings of the Second Lunar Science Conference, Geochim. Cosmochim. Acta Suppl. 2*, **1**, M.I.T. Press, pp. 617–643.
[19] Reid, A., Ridley, W., Warner, J., Harmon, R., Brett, R., and Brown, R.: 1972, *Revised Abstracts of the Third Lunar Science Conference*, pp. 640–642.
[20] Hawkins, G.: 1964, *Annual Review of Astronomy and Astrophysics*, (ed. by Goldberg, Deutsch and Layzer), Annual Reviews, Inc., Palo Alto.
[21] Gault, D.: 1970, *Radio Sci.* **5**, 273–291.
[22] McCrosky, R.: 1968, Smithsonian Astrophysical Observatory Special Report 280.
[23] Wetherill, G.: 1971, *Science* **173**, 383–392.
[24] Latham, G., Ewing, M., Press, F., Sutton, G., Dorman, J., Nakamura, Y., Toksőz, N., Lammlein, D., and Duennebier, F.: 1973, 'Passive Seismic Experiment', Sec. 9 of Apollo 16 Preliminary Science Report, NASA SP-315.
[25] Nakamura, Y. and Latham, G.: 1969, *J. Geophys. Res.* **74**, 3771–3780.
[26] Steg, R., and Klemens, P.: 1970, *Phys, Rev. Letters* **24**, 381–383.